Machine Learning Photogrammetric Analysis of Images Provides a Scalable Approach to Study Riverbed Grain Size Distributions

Peter Regier[1], Yunxiang Chen[2], Kyongho Son[2], Jie Bao[2], Brieanne Forbes[2], Amy Goldman[2], Matt Kaufman[2,3], Kenton A. Rod[2], James Stegen[2,4]

[1]Marine and Coastal Research Laboratory, Pacific Northwest National Laboratory, Sequim, WA.
[2]Pacific Northwest National Laboratory, Richland, WA.
[3]Department of Earth, Environment, and Physics, Worcester State University, Worcester, MA.
[4]School of the Environment, Washington State University, Pullman, WA.

Corresponding author: Peter Regier (peter.regier@pnnl.gov)

Key Points:

- We applied a machine learning algorithm to estimate median grain size distributions (d50) from images of river and streams.
- We compared these estimates to manual and model-based d50 estimates across the Yakima River basin.
- Photogrammetric estimates help bridge d50 knowledge gaps between manual and model-based methods.

Abstract

The distribution of sediment grain size in streams and rivers is often quantified by the median grain size (d50), a key metric for understanding and predicting hydrologic and biogeochemical function of streams and rivers. Manual methods to measure d50 are time-consuming and ignore larger grains, while model-based methods to estimate d50 often over-generalize basin characteristics, and therefore cannot accurately represent site-scale heterogeneity. Here, we apply a machine learning photogrammetry methodology (You Only Look Once, or YOLO) for estimating d50 for grains > 2 mm based on images collected from streams and rivers throughout the Yakima River Basin (YRB). To understand how photogrammetric methods may help bridge the gaps in resolution and accuracy between manual and model-based d50 estimates, we compared YOLO d50 values to manual and model-based estimates across the YRB. We found distinct differences among methods for d50 averages and variability, and relationships between d50 estimates and basin characteristics. We discuss the advantages and limitations of the YOLO algorithm versus current methods, and explore potential future directions to combine d50 methods to better estimate spatiotemporal variation of d50, and improve incorporation into basin-scale models.

Plain Language Summary

The size of sediments (e.g., rocks, pebbles, and sand) on the beds of streams and rivers control how water and nutrients move through the environment. It is helpful to know how rivers differ in sediment size in order to predict their behavior. One common method used to compare sediment sizes between different locations is to calculate average sediment size. However, measuring average sediment size across many locations is time consuming, and modeling is prone to bias. We used a computer algorithm to identify and measure all the sediments in many stream and river bed photos taken across the Yakima River basin. To test if the algorithm did a good job, we compared its output to three other methods for estimating average size across the same basin. Each method gave a different estimation of average sediment size, and we discuss the advantages and disadvantages of each.

1 Introduction

The grain size distribution (GSD) of sediments in streams and rivers, often represented by the median of the GSD (d50), plays many important roles that regulate fluvial hydrology and biogeochemistry, and their interactions. Grains ranging from clays to boulders control the locations and rates of groundwater-surface water exchange, which can influence stream metabolism, as well as gas (e.g., oxygen and carbon dioxide) and solute sources, fate, and transport (Glaser et al., 2020; Gomez-Velez et al., 2015; Harvey et al., 2011; Mori et al., 2017; Son et al., 2022; Xia et al., 2017). Because of these roles, GSD is a key metric for predicting hydraulic conductivity (J.-P. Wang et al., 2017), flow resistance (Rickenmann & Recking, 2011), microbial respiration and denitrification in streambeds (Son et al., 2022), and parameterizing hydromorphological models (Lepesqueur et al., 2019). However, constraints on accurate assessment of d50 values at the basin scale, including uncertainty and bias associated with methods used to estimate d50 and the spatially and temporally sparse nature of current d50 data, limit our ability to accurately parameterize the models used to predict key basin functions.

Historic methods for determining d50 involve destructive sampling followed by manual counting or sieving procedures (Folk, 1966; Wolman, 1954). While these methods provide direct, site-specific measurements, they are time/labor-intensive with limited reproducibility, making it difficult to provide sufficient spatiotemporal resolution needed to understand basin-scale heterogeneity of d50. Manual methods also generally favor measuring smaller grains and ignore grains over a specific size cut-off, limiting the ability to characterize large grains. Recently developed methods such as processed-based and machine learning models have been used to estimate d50 values from regional to continental scales (Abeshu et al., 2022; Gomez-Velez & Harvey, 2014; Ren et al., 2020). These methods provide the advantage of continuous spatial coverage, and eliminate the need for sample collection and analysis. However, model-based methods rely on assumed relationships that have difficulty accounting for the high heterogeneity in predictor variables at smaller (site-to-reach) scales. Moreover, differences between methods or users can lead to high variability in d50 estimates (e.g., Faustini & Kaufmann, 2007).

Recent advances in machine learning and photogrammetry hold promise for bridging the gap between manual methods, which accurately characterize d50 across a small set of samples but are difficult to scale up to basin-scale, and model-based estimates, which provide large-scale estimates at the expense of site-scale accuracy. Photogrammetric methods ingest images of sediments, and process them to estimate grain sizes, which can then be used to construct GSDs (Chang & Chung, 2012; Purinton & Bookhagen, 2019), and have been shown to agree well with manual measurement methods (Stähly et al., 2017; Steer et al., 2022). Photogrammetric methods have several advantages over manual measurements, including non-destructive sampling, higher throughput, potential to automate analyses, and improved reproducibility. In addition, as estimates are based directly on information collected at a site, photogrammetric d50 estimates are better ground-truthed to an individual sampling site than modeling approaches that must generalize based on basin-scale characteristics. Photogrammetric methods may, therefore, fill a need for improved resolution and accuracy between physical and model-based methods. However, photogrammetric methods remain sensitive to common environmental interferences to image processing such as shadows, water, and non-grain objects.

In this study, we explored how a novel machine learning photogrammetric algorithm called "You Only Look Once" (YOLO) could help overcome current method limitations used to estimate d50. YOLO presents several potential advantages over other photogrammetric approaches, including rapid image processing, robustness to common environmental interferences like shadows, static and flowing water, and non-sediment-grain objects (e.g., Detert & Weitbrecht, 2013), and initial parameterization from a collection of public datasets, reducing the model's prediction bias towards a specific location. To evaluate the utility of YOLO, we analyzed 161 images collected on the banks of streams/rivers across 40 sites throughout the Yakima River Basin (YRB, Washington, USA). We then compared YOLO estimates to manual d50 measurements and model-based d50 estimates across the YRB. By exploring similarities and differences in average values, variance, and relationships to basin characteristics, we revealed advantages and limitations of YOLO-based d50 estimation at the basin scale. Our results suggest that the YOLO algorithm is a promising high-throughput method for spatiotemporally explicit d50 estimates, and can improve site-specific accuracy and spatial resolution that limit our ability to reconcile differences between manual sampling and generalized model-based estimates. Because of the importance of accurate and spatiotemporally resolved d50 to predicting key basin processes (Son et al., 2022), our findings suggest YOLO has strong potential benefits for improving fidelity of basin-scale models.

2 Materials and Methods

2.1 Site description and image collection

We selected 40 sites spread across the YRB in southeastern Washington State, USA to represent a range of d50 values across gradients of latitude, elevation, land use, and stream order. The YRB is a 15,523 km^2 catchment characterized primarily by forests and grassland (28% and 26% respectively), as well as agriculture (15%) and a small developed footprint (3%) (Stroud Water Research Center, 2023). Our sites span the headwaters to the main stem of the Yakima River, representing 2nd-7th order streams (Figure 1). The sites capture a wide range of grain sizes from large cobbles (Figure 1B) to small rocks and finer grains (Figure 1C). We also included one image collected nearby on the Columbia River (Figure 1A).

During a sampling campaign in 2021, we collected 161 images used for estimating d50. We collected digital images of undisturbed surface sediments during the day using a 0.8 x 0.8 m white polyvinyl chloride pipe quadrat serving as the spatial reference frame. At several sites, we collected multiple images to assess intra-site variability. Original images are available through the ESS-DIVE repository (Fulton et al., 2022).

Prior to modeling, we visually assessed all images for potential environmental interferences, including shadows, wetting, sediment/biofilm obscuring grain edges, non-grain objects, and plants. Images were graded into one of four categories based on presence/absence of the above interferences: “Yes” (no substantial interference expected), “Maybe” (generally clear grains, but some potential interference”) and “No” (substantial interference expected). Grading is a subjective process and was therefore conducted by a single grader in a single session.

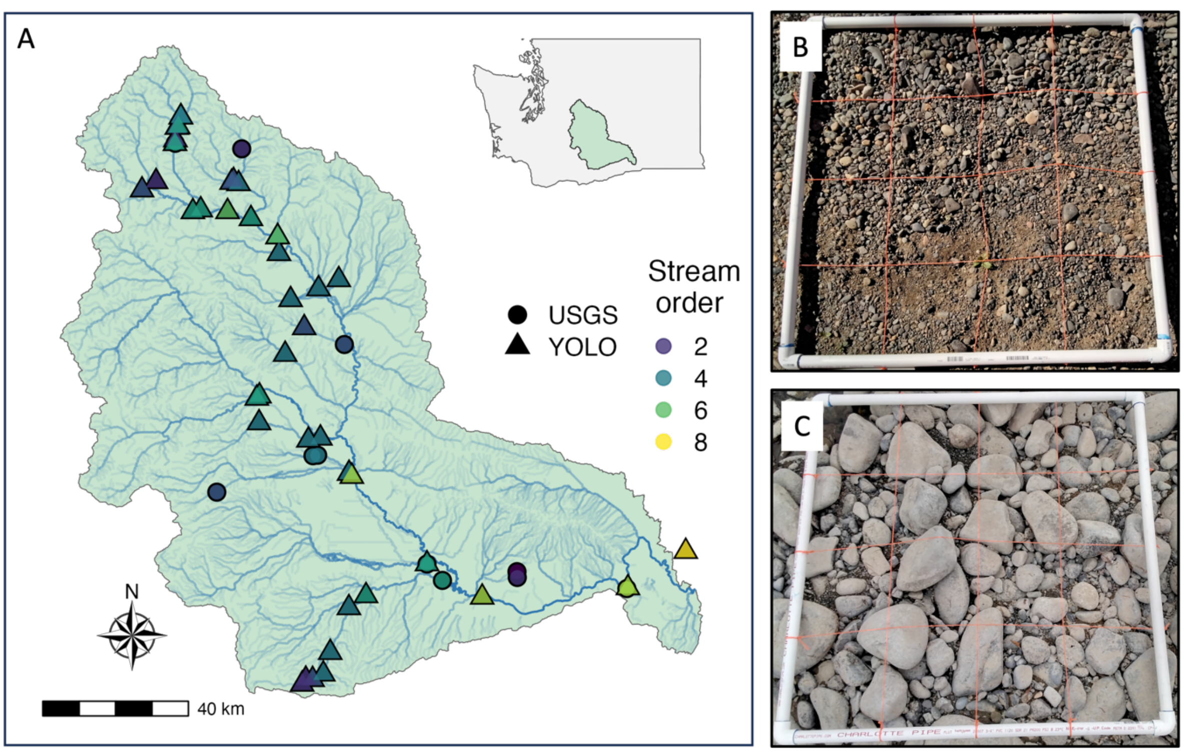

Figure 1: A) A map of the Yakima River Basin sites where images used in this study were collected. We include example photos (B and C) showing the quadrat used to define the area of

analysis where B) is an example of larger cobbles and C) is an example of smaller rocks/sand grains.

2.2 Photogrammetric d50 estimates

We selected 11 photos (10 from the YRB and 1 from a nearby site on the Columbia River, to include as many sediment geomorphological characteristics as possible) to train the You Look Only Once (YOLO, version 5) framework (Redmon et al., 2016) using code accessed from https://github.com/ultralytics/yolov5. Because speed of detection was not of concern in this study, we used the extra large-scale YOLO neural network. The structure of the YOLO neural networks are mainly connections of multiple convolutional neural networks (Zhang et al., 1990), modified bottleneck cross stage partial networks (C.-Y. Wang et al., 2019), spatial pyramid pooling fast layers (He et al., 2014), upsampling layers, and concatenated layers (https://pytorch.org/docs/stable/generated/torch.cat.html), where the full network included 476 layers and 87 million trainable parameters. We derived initial parameter values from a pre-trained network using the public YOLO COCO 128 datasets (accessed from https://cocodataset.org/). Because manually labeling individual grains within a photo for the training dataset is relatively labor intensive, we divided the training process into two steps to avoid manually labeling all 11 images. First, we selected 5 photos (4 from the YRB and 1 from the Columbia River) and manually drew bounding boxes to label individual grains (1887 grains identified). We then trained the YOLO model and updated trainable parameters, and used the trained model to label grains for the remaining 6 photos. These predicted labels were then checked and manually corrected (adding or editing delineation bounds) if grains were missing or predicted incorrectly, for a total of 4315 labeled grains in the final model. We note that YOLO implements pre-processing on the training photos, including adjusting color saturation, brightness, contrast, rotating, cutting. For each photo, we only considered the region within the quadrat, where each pixel represented a height and width between 0.22 and 0.65 mm. Using labeled grains scaled to mm, we generated GSDs, and then calculated d50 values from each GSD. These data are publicly available on the ESS-DIVE repository (Regier et al., 2023).

2.3 Manual d50 measurements and model-based d50 predictions

We gathered public data for d50 measurements made by the US Geological Survey (USGS) at 11 sites within the YRB (Figure 1) to represent manual sampling d50 values. Data were downloaded using the *dataRetrieval* R package (De Cicco et al., 2018) using parameter codes 80164-80169 which represent the percent of bed sediments passing through sieves with different pore sizes. We calculated d50 values by plotting the relationships between sieve size and percent of bed sediment, then linearly interpolating between 1) the sieve size < 50% closest to 50% and 2) the sieve size > 50% closest to 50%. Because of the limited number of sites represented for manual d50 measurements relative to YOLO and model-based predictions, we included all sites, whether co-located with YOLO sites or not, in our analysis.

We used two existing continental-scale d50 products to represent model-based d50 estimates for the YRB. The Networks with Exchange and Subsurface Storage (NEXSS) model uses d50 data from the National Rivers and Streams Assessment and the Wadeable Stream Assessment (https://www.epa.gov/national-aquatic-resource-surveys/nrsa) to predict the NHDPLUS reach-scale d50 values using a multi-linear model (Gomez-Velez et al., 2015), and we refer to these estimates as “NEXSS” from here on for simplicity. The predictor variables used by NEXSS include drainage area, channel slope, mean annual discharge, elevation and mean annual precipitation (Gomez-Velez et al., 2015). We also included d50 estimates produced by Abeshu et al. (2022), who used d50 data from 2577 USGS gage stations, and 300 locations from the U.S. Army Corps of Engineers (Gaines & Priestas, 2016; Schwarz et al., 2018), which we refer to as “Abeshu” from here on. The final predicted model used 11 predictors, including topography (basin slope, elevation, channel length, channel slope), hydro-climate (runoff, snow, aridity, wet days, temperature, and contact time), and erosion variables. We collected d50 estimates for all 40 sites used for the YOLO model for both NEXSS and Abeshu methods.

Method	Approach	Inputs	Limitations	Spatial extent
USGS	Manual sieving	sediments	grains > 2mm	point
NEXSS	Model	watershed characteristics	Model generalizations	reach-scale
Abeshu	Model	watershed characteristics	Model generalizations	reach-scale
YOLO (this study)	Photogrammetry	images	obscured/small (< 2mm) grains	0.8mx0.8m

Table 1: comparison of methods used to estimate d50 values for the YRB and methodological characteristics.

2.4 Statistics

All spatial and statistical analyses were conducted in R v4.0.5 (R Core Team, 2021). All significance tests were based on a p-value threshold of 0.05. Goodness-of-fit and error metrics for linear regression were calculated using the *hydroGOF* R package (Zambrano-Bigiarini, 2013). In order to compare the distributions of d50 values to a common distribution, we included a continental-scale d50 distribution originally presented in Figure 1d of Abeshu et al. (2022), which we first digitized (https://apps.automeris.io/wpd/), then normalized to a total count of 100 in order to scale to the magnitude of our sample size. Statistical differences between group means were assessed using Wilcoxon tests which are more robust to non-normal distributions than parametric alternatives. Correlations between variables were calculated using Spearman’s rho (r). Prior to correlation calculations, all variables were normalized using the Yeo-Johnson transformation from the *bestNormalize* R package (Peterson, 2021), which is capable of handling negative values. Spatial analysis to determine straight-line distances between sites, which we selected in preference to flowline distance for simplicity, and the main stem of the Yakima River was conducted using the *sf* R package (Pebesma, 2018). To evaluate the relationships between d50 estimates and basin/stream variables, we collected basin characteristics following methods in Gomez-Velez et al. (2015) and Abeshu et al. (2022). Variables include both basin-scale and catchment-scale versions, where basin scale represents the total upstream drainage area for each NHD stream reach and catchment scale represents the smallest NHDPLUS catchment drainage area for each NHD stream reach. We selected one land-cover metric (percent urban land cover), two catchment metrics (mean catchment elevation and catchment area), two stream characteristics (stream length and stream slope) and two climate parameters (precipitation as snow and potential evapotranspiration).

3 Results, or a descriptive heading about the results

3.1 Model performance

We first assessed the ability of our YOLO approach to estimate d50 by comparing YOLO estimates to manual integrations of grains in 10 images (excluding the image from the Columbia River) with 4229 labels representing a spectrum from dominantly small grains to dominantly large grains (determined from initial YOLO runs and confirmed visually). We assessed model performance as goodness-of-fit between training and test values using R^2 (a measure of goodness-of-fit to a least-squares regression line), where $R^2 = 0.88$ indicated relatively strong linear behavior (Figure 2A). However, the slope of the least-squares line (m = 0.72) indicated the algorithm underestimated d50 for higher values, while a y-intercept > 0 indicated that at low d50 values (< 25 mm), values were overestimated (Figure 2A). We also quantified the error associated with YOLO predictions using root mean square error (RMSE) normalized to the average d50 value. The estimated error of 17.8% is similar or smaller than uncertainty associated with other GSD estimation methods (e.g., Purinton & Bookhagen, 2019; Ren et al., 2020).

To further assess the relationship between train and test values, we subdivided each of the 10 images used in Figure 2A into 4 equally sized quadrats, and then plotted the relationship between median grain size for training and test datasets (Figure 2B). Consistent with Figure 2A, we observed strong goodness-of-fit ($R^2 = 0.89$), slightly smaller error (RMSE = 16%), and a similar slope (m = 0.79) and intercept (b = 5.59). The similarity in these relationships indicated that the YOLO model performed well on both data treatments (whole image d50 and median grain size of image subsets).

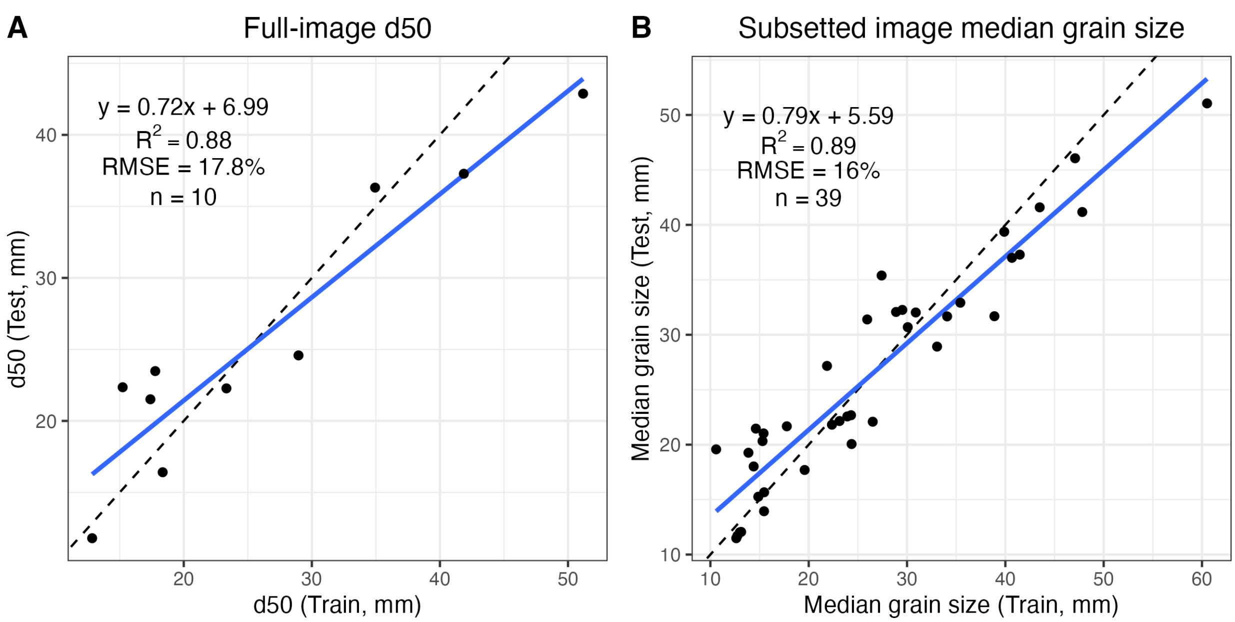

Figure 2: A) Comparison of manual estimates ("Train") versus YOLO algorithm estimates ("Test") of median grain size distribution (d50) from 10 photos that represent a spectrum of d50 values within our dataset. Goodness-of-fit is presented as R^2, while error is presented as root mean square error (RMSE). B) Comparison of manual and YOLO-derived estimates for image subsets (images were divided into 4 subsets based on mean x and y pixel coordinates, and then

median grain size was calculated. We note that one outlier was removed from B), but is shown along with the corresponding image extent in Figure S1.

3.2 Comparison to existing d50 estimates

Figure 3 compares the four methods used to measure or estimate d50 across the YRB (Table 1). We observed significant (p-values < 0.05) differences in median d50 values (Figure 3A), with the difference between YOLO and NEXSS being the least significant ($p = 0.025$), while all remaining comparisons were highly significant ($p < 0.0001$). YOLO d50 estimates were highest, followed by the two model-based methods, and USGS d50 measurements having the lowest mean d50 (mean d50 values of 24.2, 21.4, 1.2, and 0.2 mm, respectively). Variance also differed markedly between estimation methods, with standard deviations of 8.9, 26.9, and 0.7, and 0.2 for YOLO, NEXSS, Abeshu, and USGS, respectively.

To better understand how distributions of d50 produced by each estimation method compare, we plotted estimates for the YRB relative to a distribution of d50 values collected from 2577 stations presented in Abeshu et al. (2022) across the continental US (CONUS) in Figure 3B. We note that while the continental-scale distribution represents a wide range of elevations and gradients, the YRB is composed primarily of high-gradient, high-elevation streams (Figure S2). As such, we expected that YRB sites would have larger grains relative to the continental-scale distribution. All methods except USGS skewed to the right relative to the CONUS distribution, while USGS measurements skewed left (Figure 3B). Both Abeshu and YOLO estimates followed generally unimodal distributions, while USGS estimates did not follow a clear distribution (likely due to limited sample size), and NEXSS estimates represented a generally bimodal distribution, with notable outliers at very small d50 values, with a minimum value of 0.005 mm (5 µm), which was well below the lower limit of the CONUS distribution.

We next explored how each method's estimates changed with stream order (Figure 3C). Based on geomorphology, we expected that lower-order streams would generally have larger grains, and that grain size would generally decrease as stream order increased due to downstream fining (e.g., Menting et al., 2015). Consistent with this theory, the highest stream order corresponded to the lowest d50 values for all methods with the exception of USGS, which showed a general increase in d50 from lowest to highest stream order. However, we did not observe consistently monotonic relationships across stream orders 2-6 for any of the methods (Figure 3C). For Abeshu and YOLO, we observe decreasing trends from stream order 2 to stream order 4, then increasing d50 values from stream order 4 to stream order 6. In contrast, NEXSS estimates show increasing d50 values from stream order 2 to 5, and then a decrease from 5 to 6. Similar to Abeshu, USGS d50 values showed a U-shaped pattern from 2nd to 5th order streams (Figure 3C).

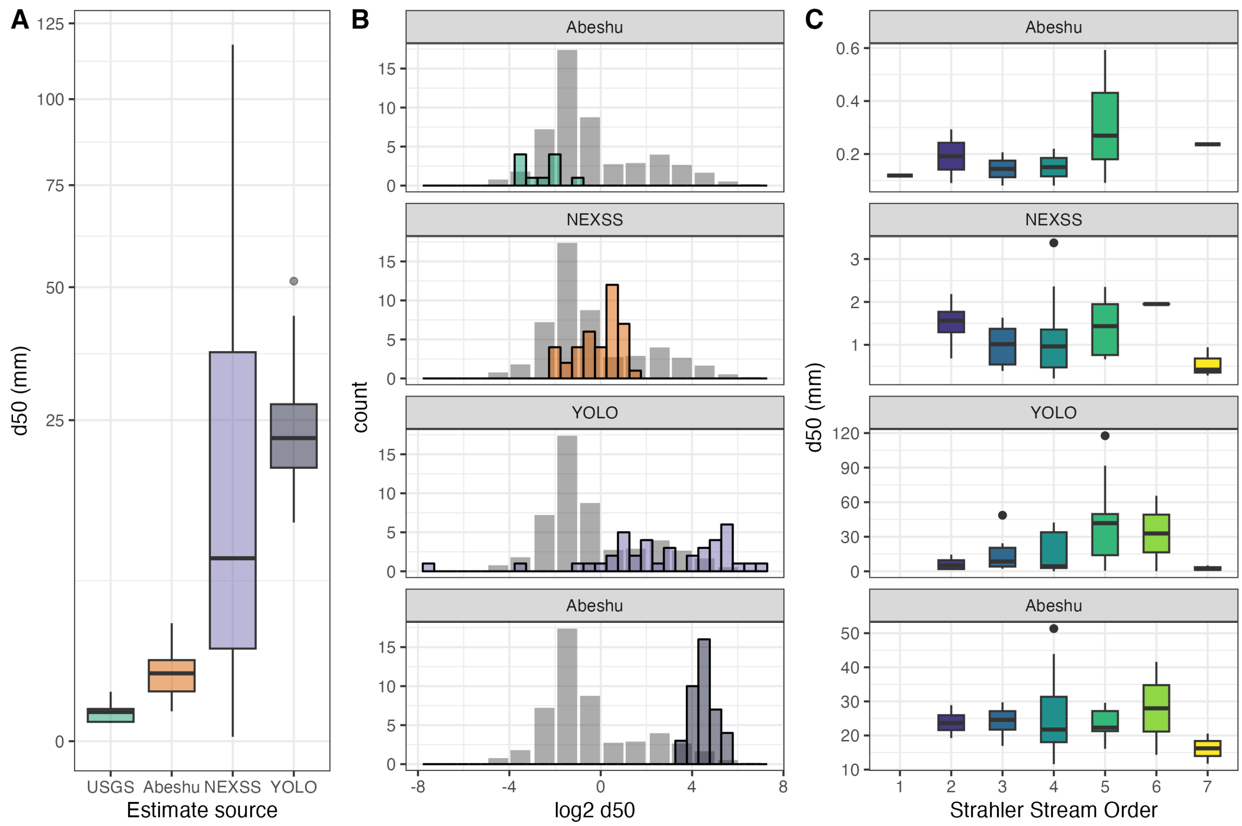

Figure 3: Comparison of YOLO estimates across the YRB to three other measurement/estimation methods. A) d50 values compared between four methods, B) a comparison of the distribution of four methods to a standard distribution of d50 measurements (gray bars) from across the continental US, originally presented in Abeshu et al. (2022), and C) a comparison of d50 estimates from each method grouped by stream order (Note: vertical axes are different scales).

Finally, we explored how d50 estimates varied spatially across the YRB (Figure 4). All methods presented different spatial patterns, which we visualized as above and below median values for simplicity. Higher (above median) Abeshu d50 estimates generally clustered in the northern part of the basin, but also along the Satus tributary in the southwest. Similarly, higher NEXSS d50 values cluster consistently in the northern half of the basin, with highest values clustered along the northernmost tributary sampled. In contrast, YOLO estimates were spatially distributed, with highest d50 values on tributaries in the middle of the basin. Consistent with Figure 3C, the 7th order site located in the far southeast corner of the basin is below median for both model-based methods and YOLO, but is above median for USGS.

To quantitatively explore these relationships, we compared differences in latitude, longitude, and straight-line distance from the main stem of the Yakima for all sites in Figure 4 between above-median and below-median d50 values (Figure S3). For distance from the Yakima, YOLO was the only method of the four that showed significant differences ($p = 0.026$) between above-median and below-median values (Figure S3), where above-median d50 sites were considerably farther from the main stem of the Yakima River (median: 16.3 km) compared to below-median d50 sites (median: 1.8 km). For both Abeshu and NEXSS, above-median d50 values were located at more northern latitudes and more western longitudes (all p-values < 0.05). Neither YOLO nor USGS d50 values showed significant relationships to latitude or longitude (Figure S3).

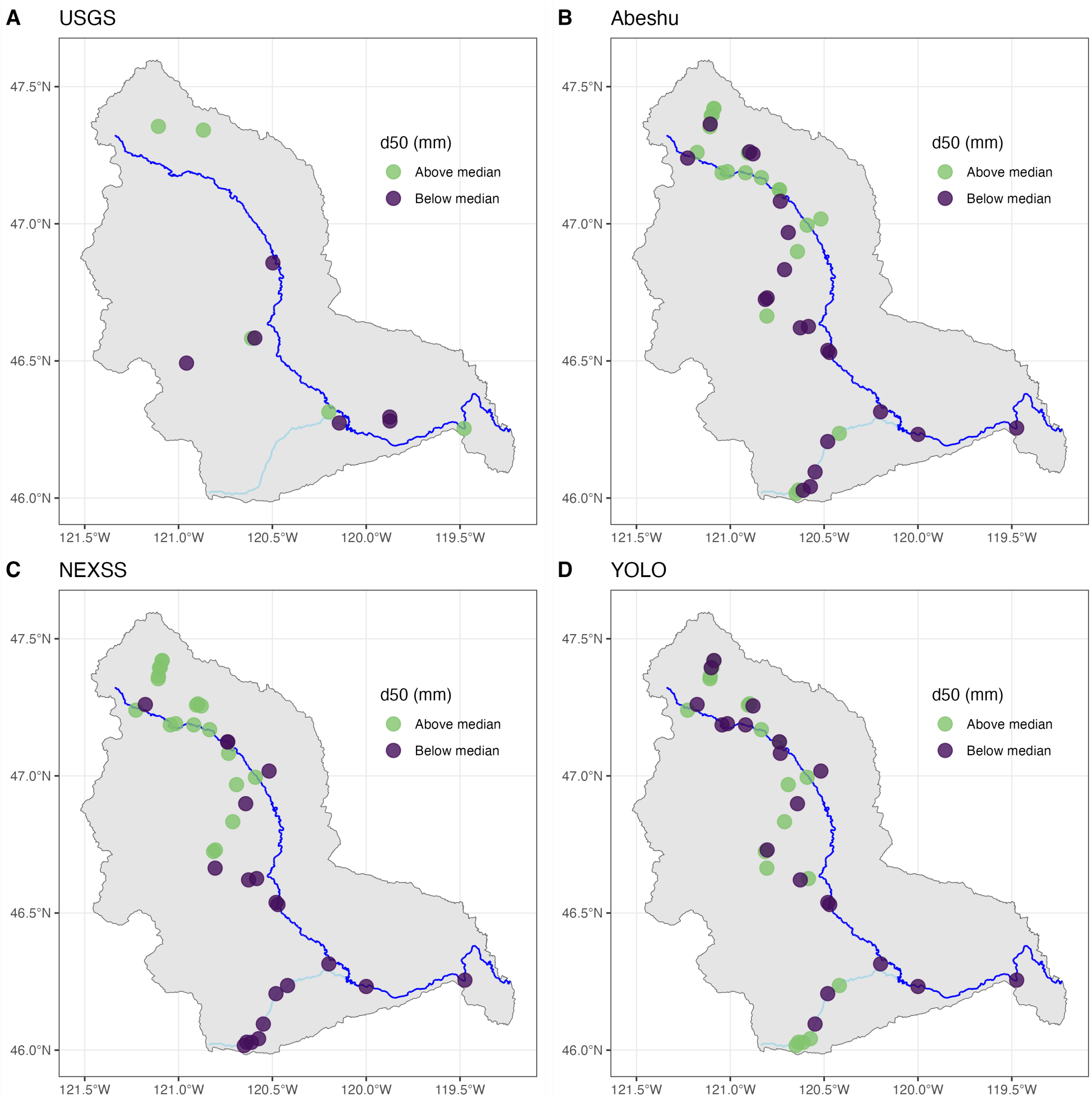

Figure 4: Comparison of d50 methods. For USGS, all sites available within the YRB were used, while for NEXSS and Abeshu, sites match study sites used for YOLO estimations. Note that medians are determined separately for each method. For reference, the main stem of the Yakima River is plotted in dark blue, and Satus Creek is plotted in light blue

3.3 Correlations to basin characteristics

To better understand how d50 estimates related to each other and catchment properties, we examined correlations between d50 estimates and basin characteristics (Figure 5). Because the USGS d50 dataset has a much smaller sample size and many sites were not co-located with the other three methods, they were excluded from this analysis. Since we were interested in understanding how the scale of environmental characteristics relates to each d50 estimation method, we separately explored correlations to environmental characteristics computed at the basin-scale (Figure 5A), and the same environmental characteristics, but calculated at catchment resolution (Figure 5B). We note that the basin-scale and catchment-scale are defined in the Methods. Among the three d50 estimation methods, we observed the strongest correlation between Abeshu and NEXSS ($r = 0.25$), while correlations to YOLO were weaker ($r = 0.04$ and 0.09 respectively). This is not surprising as Abeshu and NEXSS methods estimated using large-scale modeling approaches (Table 1).

At the basin scale (Figure 5A), NEXSS exhibited the strongest correlation to evapotranspiration ($r = 0.72$) and strong correlations ($r > |0.5|$) to all catchment variables except for basin area and stream length. Abeshu correlations were weaker, with the strongest correlation to precipitation as snow ($r = 0.63$), but generally showed the same patterns (i.e., correlations are positive for both methods or negative for both methods). In contrast, the strongest correlation for YOLO was basin area ($r = -0.27$), and several variables that strongly co-varied with both NEXSS and Abeshu d50 estimates (stream slope, precipitation as snow, and potential evapotranspiration) showed considerably weaker correlations to YOLO ($r < |0.15|$).

For catchment-scale characteristics (Figure 5B), the strongest correlations for NEXSS and Abeshu were weaker ($r = -0.56$ and -0.49, respectively), while the strongest correlation for YOLO was stronger ($r = -0.34$). Both NEXSS and Abeshu exhibited weaker correlations to all variables except basin area and stream length. We observed the largest decrease in correlation between basin-scale and catchment scale for NEXSS in urban land cover (from $r = -0.61$ to $r = -0.17$) and for Abeshu in stream slope (from $r = 0.40$ to $r = -0.04$). Strong correlations between NEXSS and precipitation as snow, mean elevation, and evapotranspiration are linked to precipitation and elevation as predictor variables used for d50 estimates (Gomez-Velez et al., 2015). Similar correlations to between Abeshu estimates and snowfall are also expected, as snowfall was identified as a key predictor in their model (Abeshu et al., 2022), and snowfall correlates strongly with both mean elevation and evapotranspiration (Figure 5). For YOLO, correlations to catchment-scale variables were stronger for urban land cover, stream slope, precipitation as snow, and potential evapotranspiration.

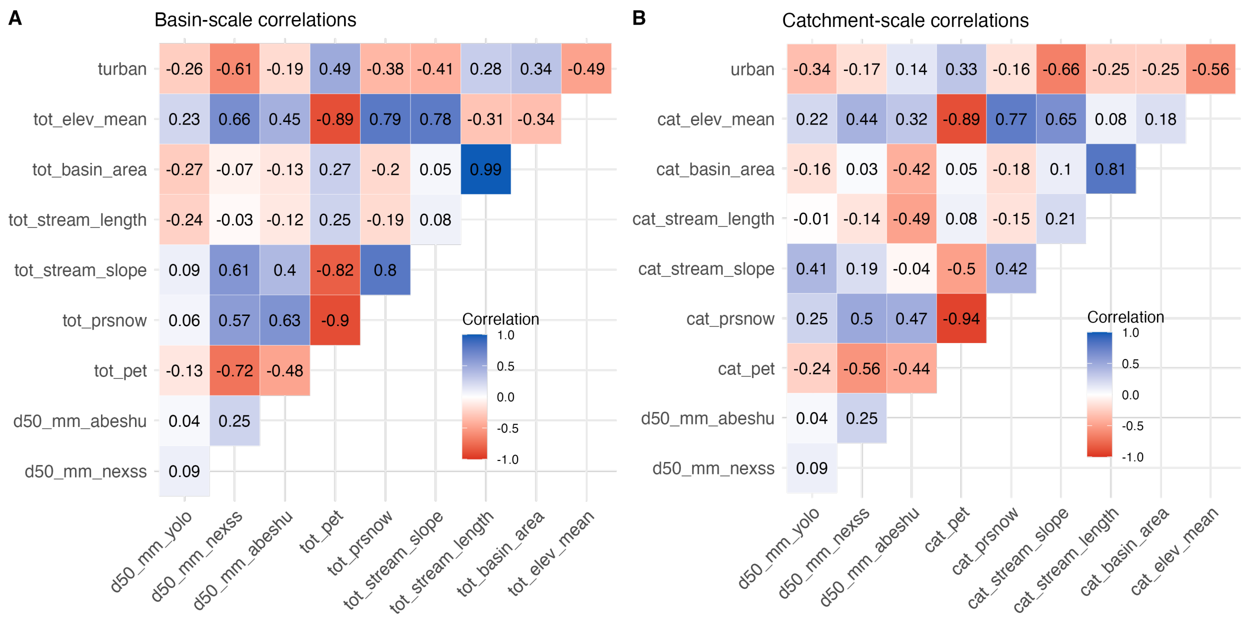

Figure 5: Spearman correlations (presented both as colors and numbers inside each box) between the three methods for estimating d50 values for the YRB in Figure 3 and catchment characteristics (urban = % urban land cover, elev_mean = mean catchment elevation, prsnow = precipitation as snow, and pet = potential evapotranspiration). Prefixes indicate basin-scale ("tot") or catchment-scale ("cat") where applicable.

3.4 Intra-site variance in YOLO estimates

To better understand intra-site variability in YOLO d50 estimates, we calculated means and standard deviations for 12 sites with at least 6 images (Figure 6). To directly compare across sites with different numbers of images, we calculated the means and standard deviations for 1000 random selections of 5 images from each site, and Figure 6 reports the mean of each statistic (mean and standard deviation) across the 1000 calculations within each site. Standard deviations for each site represent intra-site variability, while standard deviation of all images ("All") represents inter-site variability within our dataset. For several sites, intra-site variability was larger than inter-site variability (Figure 6A). Because mean values differ widely across the sites in Figure 6A, we normalized standard deviations to mean values in order to directly compare intra-site and inter-site variability (Figure 6B). Based on this analysis, several sites, most notably S15, exhibited higher intra-site variability than the inter-site variability within our dataset.

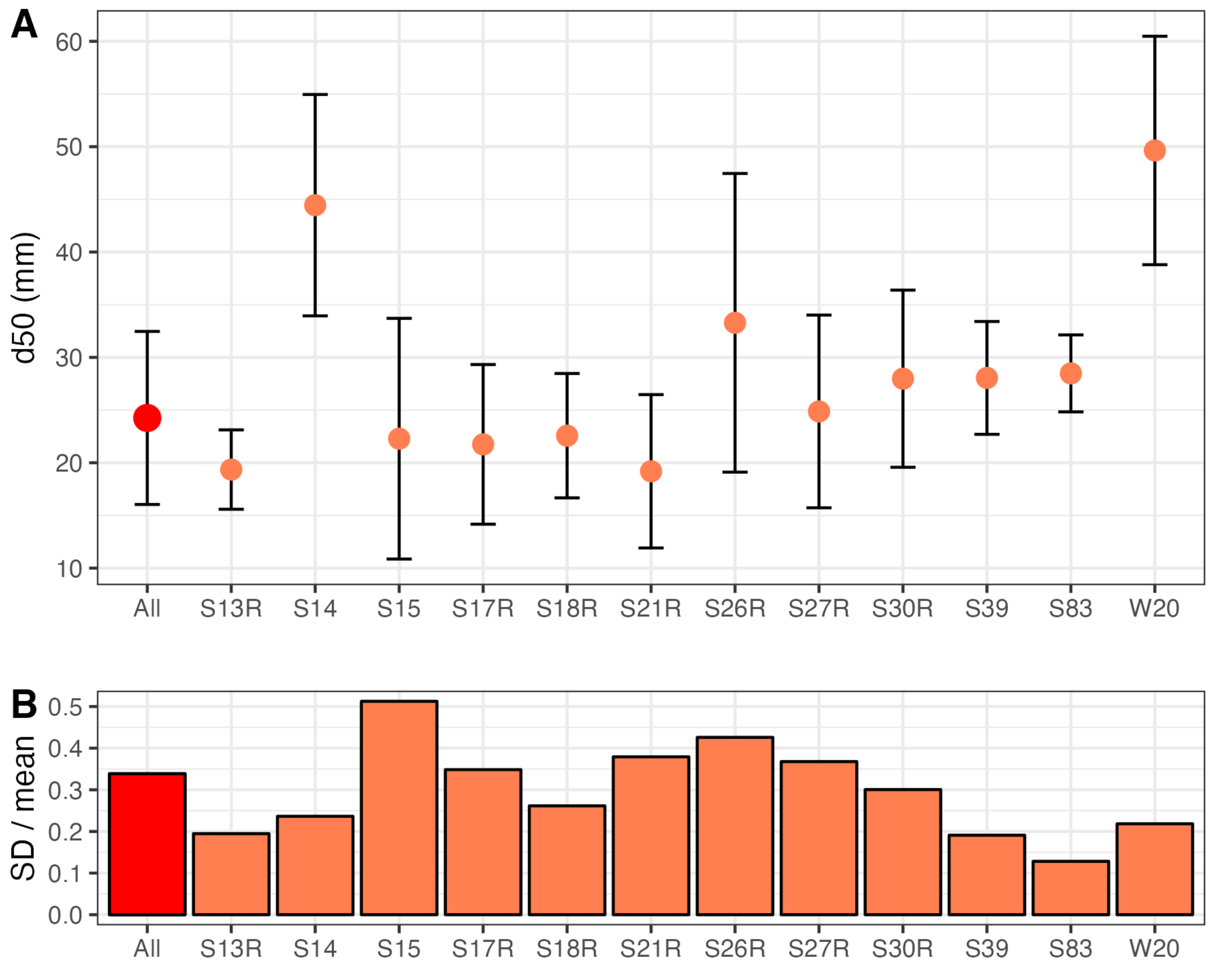

Figure 6: A) Intra-site variability for study sites with n > 5 images presented as mean values (dots) +/- standard deviation (upper and lower error bars, respectively). Mean and standard deviations are calculated as the average of 1000 random selections of 5 images within a site (or across the full dataset for "All"). B) We also present standard deviations divided by means to fairly compare variability between sites.

3.5 YOLO image grading

Prior to YOLO modeling, we manually assessed all images for suitability, as described in the Methods, with an average labor burden of 30 seconds per image. In order to understand how useful this grading process was, we explored the relationship between assessment by the human eye and YOLO's internal accuracy in Figure 7. We found that images deemed unsuitable for modeling (Image suitability = "no") had significantly ($p < 0.0001$) lower accuracy (mean = 54%) relative to images deemed potentially suitable ("maybe") and suitable ("yes"), with mean accuracies of ~63% and 64%, respectively.

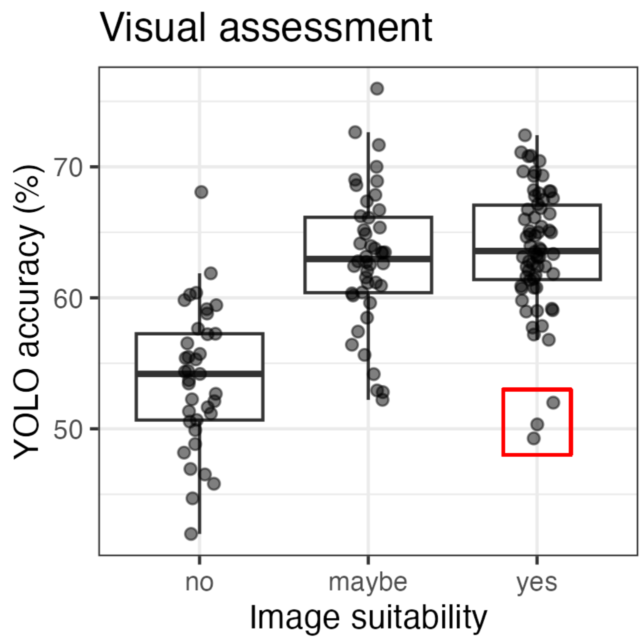

Figure 7: All images used to parameterize the YOLO model were first visually assessed for modeling suitability, as explained in the methods. Image suitability is plotted against YOLO's internally reported accuracy metric for grain identification for each image. The red box delineates three potential "yes" outliers presented in Figure S4.

However, we also noted 3 outliers graded "yes" with accuracies below 55% (red box in Figure 7). To better understand the discrepancy between visual assessment and YOLO performance as a potential limitation of the YOLO method, the three images are presented in Figure S4. For Photo A, the average grain size of 0.49 mm was similar to the resolution of the image (0.3-0.4 mm/pixel). Since the YOLO model needs at least 8 pixels to correctly detect a grain, we attribute the low accuracy for Photo A to the insufficient photo resolution. Similar to Photo A, Photo B has a number of very small grains, less than 8 pixels that were not identified by the YOLO algorithm. The 279 grains detected represent 5.7% of this image, indicating that the majority of grains within the image were not identified. Photo C, similar to Photos A and B, was largely composed of very small grains that are difficult for YOLO to resolve as they approach the resolution threshold of the image. Additional potential interferences in Photos B and C include non-grain objects (grass and sticks) and shadows. However, we note that grains were identified in Photo B in both shaded and sunny portions of the image, suggesting that shadows were not a significant interference in grain identification for the image.

4 Discussion

4.1 Comparability of image-based and model-based d50 estimates

Our comparison of varying d50 measurement/estimation methods found that each method gave different interpretations of d50 values, their distributions across the study area, and their relationships to basin characteristics. Because the USGS dataset is the only method presented that measures d50 instead of estimating it, we suggest that these values represent "ground-truth" for d50 values in the YRB, with caveats that USGS sites are not co-located with YOLO sites, the sample size is limited, and values are constrained by a maximum grain size threshold of 0.2 mm

(Table 1). As expected based on minimum grain size (Table 1), mean d50 values were significantly ($p < 0.05$) higher for the photogrammetric method (YOLO) relative to our understanding of ground-truth (USGS measurements). We expected NEXSS and Abeshu measurements to have similar mean d50 values as USGS because neither model-based method includes a size cut-off (Table 1). However, both methods had significantly ($p < 0.0001$) higher mean d50 values, indicating that both methods overestimated d50 across the YRB relative to our understanding of ground-truth. Figure 3B indicates some overlap between USGS and Abeshu, and considerably less overlap with NEXSS, indicating that Abeshu estimates are more closely aligned with the true magnitude of d50 across the YRB than YOLO or NEXSS estimates.

NEXSS estimates also had the highest variance across the basin of the three methods (Figure 3A), which is somewhat surprising as we anticipated that process model-based estimates would vary less than photogrammetric and manual estimates. In addition, NEXSS estimates are based on a series of empirical relationships, while both Abeshu and YOLO estimates are derived from machine learning algorithms without explicit boundary conditions, which we anticipated would result in lower variance for NEXSS estimates. Instead, we found that standard deviations were smaller than mean values for both YOLO and Abeshu, but the NEXSS standard deviation was larger than its mean (Figure 3A). We interpret this as NEXSS being more sensitive to a wide range of environmental conditions represented across the YRB relative to Abeshu. Both Abeshu and YOLO methodologies use localized data inputs (relationships based on local basin characteristics and local images, respectively), while NEXSS uses relationships established at a continental scale. In addition, while NEXSS is well-validated in lower-relief catchments (Gomez-Velez et al., 2015), it has been suggested that the methodology may not represent headwater streams accurately (e.g., Ward et al., 2019). Thus, we infer that higher variance from NEXSS estimates is related to a combination of being based on larger scale (and thus less specific) relationships and the prevalence of high-relief locations in this study, for which NEXSS may perform poorly. Our results highlight the benefit of utilizing multiple d50 estimation methods, ideally in concert with manual measurements to ground-truth. For models that depend on d50 to parameterize important basin processes like respiration (Son et al., 2022), based on results in Figure 3, we would expect dramatically different process estimates based on each d50 method, with more variable estimates from NEXSS than the other three methods.

We also found differences across estimation methods in the relationships between d50 and stream order (Figure 3C). Based on basin hydrology and geomorphology, we expected that increasing stream order would correlate to lower slope, and therefore decreasing velocities, meaning higher order streams should have smaller d50. While d50 values were generally lowest at the largest stream order, each method exhibited a unique pattern for stream orders 1-6. The lack of a monotonic decreasing trend is particularly surprising for NEXSS and Abeshu estimates, which are both modeled using catchment properties, and correlate to basin-scale parameters (elevation, stream slope, and precipitation, Figure 5A). Instead, we suggest that deviation from the expected trend can be explained by the complex suite of factors that influence fining across basins, including underlying geology, stream gradient, channel width, and discharge (Church, 2002; Menting et al., 2015). We note that all methods show increased variance in mid-order streams, which is likely partially due to larger sample sizes, but also may be associated with wider variance in site characteristics for these sites (e.g., Figure S2). The lack of a clear trend between d50 and stream order is also consistent with other studies, which found a similar divergence from expected spatial patterns (Menting et al., 2015; Snelder et al., 2011; Splinter et al., 2010), although expected patterns of fining of grains have been observed in lower-relief systems (e.g., Costigan et al., 2014).

Further exploration of the spatial trends in d50 values (Figure 4, Figure S3) identified both latitude and longitude as significant covariates for d50 estimates for Abeshu and NEXSS methods, indicating spatially structured controls that may be unrelated to stream order. These results suggest that modeled d50 estimates (Abeshu and NEXSS) follow broader spatial patterns within the basin. Due to lack of relationships to latitude or longitude for USGS and YOLO d50 datasets, we suggest these methods are more sensitive to local controls (Figure S3). For YOLO, this is supported by stronger correlations to catchment-scale variables relative to basin-scale variables (Figure 5), and a significant relationship to a site's distance from the main stem (Figure S3). This is consistent with the scales at which the four methods operate, with both Abeshu and NEXSS taking "top-down" views, where d50 estimates are built on continental-scale frameworks which are down-scaled to the site scale, while the USGS method and YOLO algorithm only access site-specific information, and are therefore unaware of, and theoretically independent of basin properties.

Together, our results suggest that continental-scale relationships that work for continental-scale modeling of d50 may not be sufficient for modeling at site-to-catchment scales where the generic physical rules do not apply consistently enough to provide trustworthy d50 predictions. As such, methods that incorporate site-scale information (e.g. manual or YOLO) are needed to provide accurate d50 data to hydro-biogeochemical models. That is, potential error associated with continental-scale d50 predictions may lead to erroneous site-scale predictions of river corridor function due to the dominant role of physical properties like d50 on both hydrologic and biogeochemical function (e.g., Son et al., 2022).

4.2 Advantages of photogrammetry estimation

We found YOLO to be an effective method for estimating d50 values (Figure 2) for grains larger than pixel resolution (~2mm, as reported by the YOLO algorithm for images used in this study), ranging from sand/gravel to cobble (Figure 1). The maximum grain size evaluated here is not tied to YOLO itself, but rather the way in which photos were taken. For example, photos taken from further off the ground (e.g., via drone) could be analyzed by YOLO to capture larger grains (e.g., boulders). Below, we identify some advantages associated with this method.

One clear advantage of the YOLO approach is the lack of external data required for d50 estimations. Unlike model-based approaches, which are subject to the spatial resolution of input variables, YOLO determines d50 values solely based on an image. In areas with sparse data coverage (e.g., ungauged catchments), model inputs are based on remotely sensed data with minimal ground-truthing, which can lead to bias and large uncertainty of the input variables (Abeshu et al., 2022; e.g., Gomez-Velez et al., 2015). YOLO stands as a promising complementary method, as stream/river access is not required (as for manual sample collection), and results will be as accurate in an ungauged catchment as a heavily instrumented research basin. With advancements in both photography and aerial drone technologies, we see great potential for collecting many images to spatially characterize d50 values across reach-to-basin scales, as explored in other studies (e.g., Lang et al., 2021). In addition, the coupling of YOLO with an uncrewed approach could prove a powerful yet safe way to estimate d50 in hard-to-access locations, or during unsafe field conditions. We also see potential for videographic application of the YOLO algorithm, which can process 45-115 frames per second (Redmon et al., 2016), and could therefore potentially provide near real-time d50 estimates. This capability allows for spatially resolved estimates over a short period of time, but also facilitates rapid rescanning of d50 estimates, which could be applicable to collecting high-frequency assessments useful for understanding event-scale (storms, ice-out, etc) shifts in geomorphology (Lin et al., 2014; Tremblay et al., 2014). In addition, because of the speed with which YOLO processes images, the internal accuracy metric derived for each photo (Figure 7) could be used to assess image suitability for modeling in real-time, allowing operators to adjust the mission (changing altitude, flight paths, etc) to improve data quality, and potentially indicate when a site has been sufficiently characterized.

Another advantage of YOLO is the ease of collecting large datasets. Unlike manual methods, where each sample requires permission to destructively sample, time in the field to collect, and time in the lab to prepare, analyze, and clean up, the major limitation on the sample size of photos collected for YOLO estimates is the ability to collect a suitable image. Because of this, it is feasible to characterize the average value and variability of d50 at a site simultaneously by collecting multiple images at every site and then calculating d50 values for each image.

The high intra-site variability for S15 and S26R in Figure 6 highlights the importance of this capability. To illustrate the causes of high variability, Figure S5 presents six images all taken at the same site (S15), all taken within approximately 100 m of each other on the same river reach, which represent a gradient of grain size distributions from primarily sand/gravel to boulders that take up almost the entire quadrat. By accurately representing this level of intra-site variability, YOLO presents an opportunity to bridge the gap between manual sampling and modeling estimates, where a virtually unlimited number of photos can be analyzed with minimal additional effort to provide rapid and robust d50 estimates to quantify both median and variance. As mentioned above, incorporation of automated image collection via drones or other technologies would extend this capability from a single site to spatially resolved reach-scale profiles, and incorporating edge computing capabilities could provide estimates of data quality and indication of sufficient data collection “on-the-fly”.

4.3 Limitations of photogrammetry estimation

While YOLO provides several advantages, as described above, there are also limitations to this method relative to manual and model-based approaches. First, only surface sediments are captured, while manual methods can characterize sediments at depth. An additional limitation is the method is only as good as the image collected. As an example, Figure S6 presents two images where the YOLO algorithm does not capture all grains within the reference frame. On the top row, while most grains are accurately identified, a large grain in the upper left is partially outside the frame, and therefore is not identified. The bottom row presents an extreme example of this, where two large grains (boulders) dominate the frame, and neither is identified by the algorithm. For these cases, the YOLO algorithm would need either additional training, flexibility, or potentially manual review after grain assignment to more accurately represent d50 values.

As YOLO is an image processing algorithm, it is inevitably designed to emulate human vision, so it is not surprising that visual assessment via the human eye relates to the algorithm’s accuracy (Figure 7). However, the significant distinction between “no” and “maybe”/”yes” highlights the value of this brief visual inspection prior to modeling. Although this quality control pre-processing is a current limitation of the YOLO method, we suggest that future iterations of the YOLO approach could help develop a “living model” that continually learns and improves grain identification by ingesting new images then rerunning. The ability of this living model to automatically detect unsuitable images is supported by the relationships we observed between human-assigned image suitability and machine-assigned YOLO accuracy (Figure 7). , which is supported as the algorithm ingests a larger and more diverse set of images.

To address insufficient resolution issues for small grain size identified by Figure S4, we suggest a combination of increased image resolution and quadrat size scaling such that the majority of grains occupy at least 8 pixels. Our current approach limits our resolution to ~2mm grains and larger, making it useful in gravel/cobble-dominated streams. However, using a higher-resolution imaging system would improve the ability to resolve smaller grains. In heterogeneous catchments, we suggest carrying multiple, clearly labeled quadrats as a simple and cheap solution that would likely significantly improve YOLO performance by largely eliminating the issues identified in Figure S4. We also note that, because quadrats are placed manually, utilizing best practices for random sampling (e.g., randomly selecting cells from a grid) is important to protect against sampling bias.

4.4 Future directions

We see great potential for the YOLO algorithm to be incorporated into a living model that 1) ingests new images supplied via a simple interface (potentially via a publicly available app supporting crowdsourced input), 2) automatically assesses image quality and variability as photos are taken, and 3) reruns the model incorporating the new information. As mentioned above, this opens an opportunity for real-time quality control during data collection in the field, simultaneously improving YOLO model fidelity, optimizing image-capture field efforts (e.g., informing investigators when enough images have been collected to sufficiently represent the study site or system), and eliminating the need to manually assess image quality prior to modeling. This edge computing approach to data-model integration would ensure that high-quality data are collected for all sites via real-time quality control, eliminating site loss due to image issues, which was a limiting factor to the accuracy of the YOLO model in this study (Figure 7). Coupled with technologies for imaging large spatial scales like drones, a living YOLO model could rapidly expand from site to catchment and basin-scale d50 estimates.

Because of the ability of YOLO to quickly estimate d50 from images, we suggest that YOLO holds the potential to bridge the gap in spatiotemporally resolved d50 estimates between site-specific (manual) and over-generalized model-based approaches. As an example, in the YRB, manual d50 estimates are available, but at a limited number of locations and over limited time-scales that make extrapolation difficult. Likewise, as discussed above, model-based estimates can be down-scaled to individual reaches, but are over-generalized due to the coarser resolution of their input parameters and can be biased by basin features (e.g., a model parameterized in low-relief systems exhibits high variability in our high-relief basin). Our YOLO estimates provide site-specific information at a larger number of sites than the manual estimations, but are not biased by model constraints or input parameter resolution. As such, exploring the differences and similarities between 1) YOLO and co-located or co-collected manual measurements, and 2) YOLO and model-based measurements could provide basin-specific calibration of models capable of reconciling the accuracy of direct measurements with the spatiotemporal resolution of model-based estimates. While these relationships would be basin-specific, additional YOLO campaigns in other, contrasting basins with manual and model-based estimates would move towards basin-agnostic relationships.

YOLO estimates across multiple basins, incorporated into an iterative, living model could then be scaled up to provide continuous spatial coverage of d50 estimates required to parameterize basin-scale model data needs. We see potential for such an approach, utilized within a data-model feedback loop like the Model-Experiment (ModEx) framework (Serbin et al., 2021) to iteratively identify locations of high uncertainty for d50 estimates across a region of interest, which can help target data collection for improving YOLO models. In turn, because hydro-biogeochemical models depend on d50 for parameterization, iterative improvement of d50 products would iteratively improve model performance, better constraining estimates of key basin functions like sediment respiration (Son et al., 2022).

5 Conclusions

In this study, we explored how estimates of median GSD (d50) derived from four different methods varied across 40 sites within the Yakima River Basin. Photogrammetric methods (YOLO in this study) bring advantages of rapid throughput, low sample cost, and site-specific information, which complement both manual and model-based methods, which are limited by low throughput and over-generalization, respectively. In addition, YOLO can easily estimate intra-site variance, which is difficult with manual methods, and not possible for the model-based methods explored here. As such, we suggest that photogrammetric methods hold bridge the gap between “bottom-up” site measurements and “top-down” model-based estimates towards spatially and temporally resolved, scalable estimates of GSD (both median and variance). The flexibility of the data input (images of sufficient quality with some physical reference) and the speed of the YOLO method are primed for use on uncrewed platforms, inclusion in citizen or crowdsourced science campaigns, and ingestion of existing high-resolution datasets to rapidly improve the coverage and resolution of ground-truthed GSD estimates from reach to continental scales. We envision this coalescence of data as a living model that maintains site-specific accuracy while scaling predictive capabilities up to regional or continental scales as more data from an increasingly broad range of ecosystem types and geographic regions are ingested. Using this constantly improving d50 product, in concert with manual and model-based d50 values, we see strong potential to iteratively improve d50 representation in models improving both quantitative (magnitude) and qualitative (spatial and temporal organization) estimates of basin-scale hydro-biogeochemical processes.

Acknowledgments

We gratefully acknowledge members of the larger River Corridor Science Focus Area team who collected the field images used for modeling, including Morgan Barnes, Mikayla Borton, Stephanie Fulton, Samantha Grieger, Sophia McKever, Opal Otenburg, Lupita Renteria, and Joshua Torgeson. This research was supported by the U.S. Department of Energy (DOE), Office of Biological and Environmental Research (BER), Environmental System Science (ESS) Program as part of the River Corridor Science Focus Area (SFA) at the Pacific Northwest National Laboratory (PNNL). PNNL is operated by Battelle Memorial Institute for the DOE under Contract No. DE-AC05-76RL01830. The authors declare no conflict of interest.

Open Research

Data used in this manuscript are publicly available on ESS-DIVE at https://data.ess-dive.lbl.gov/view/doi:10.15485/1972232 and R code is available on Github at https://github.com/peterregier/d50_computer_vision.

References

Abeshu, G. W., Li, H.-Y., Zhu, Z., Tan, Z., & Leung, L. R. (2022). Median bed-material sediment particle size across rivers in the contiguous US. *Earth System Science Data*, *14*(2), 929–942. https://doi.org/10.5194/essd-14-929-2022

Chang, F.-J., & Chung, C.-H. (2012). Estimation of riverbed grain-size distribution using image-processing techniques. *Journal of Hydrology*, *440–441*, 102–112. https://doi.org/10.1016/j.jhydrol.2012.03.032

Church, M. (2002). Geomorphic thresholds in riverine landscapes. *Freshwater Biology*, *47*(4), 541–557. https://doi.org/10.1046/j.1365-2427.2002.00919.x

Costigan, K. H., Daniels, M. D., Perkin, J. S., & Gido, K. B. (2014). Longitudinal variability in hydraulic geometry and substrate characteristics of a Great Plains sand-bed river. *Geomorphology*, *210*, 48–58. https://doi.org/10.1016/j.geomorph.2013.12.017

De Cicco, L. A., Hirsch, R. M., Lorenz, D., & Watkins, D. (2018). *DataRetrieval* [Computer software]. U.S. Geological Survey. https://doi.org/10.5066/P9X4L3GE

Detert, M., & Weitbrecht, V. (2013). *User guide to gravelometric image analysis by BASEGRAIN*.

Faustini, J. M., & Kaufmann, P. R. (2007). Adequacy of Visually Classified Particle Count Statistics From Regional Stream Habitat Surveys1. *JAWRA Journal of the American Water Resources Association*, *43*(5), 1293–1315. https://doi.org/10.1111/j.1752-1688.2007.00114.x

Folk, R. L. (1966). A Review of Grain-Size Parameters. *Sedimentology*, *6*(2), 73–93. https://doi.org/10.1111/j.1365-3091.1966.tb01572.x

Fulton, S. G., Barnes, M., Borton, M. A., Chen, X., Farris, Y., Forbes, B., Garayburu-Caruso, V. A., Goldman, A. E., Grieger, S., Kaufman, M. H., Lin, X., McKever, S. A., Myers-Pigg, A., Otenburg, O., Pelly, A., Ren, H., Renteria, L., Scheibe, T. D., Son, K., … Stegen, J. C. (2022). *Spatial Study 2021: Sensor-Based Time Series of Surface Water Temperature, Specific Conductance, Total Dissolved Solids, Turbidity, pH, and Dissolved Oxygen from across Multiple Watersheds in the Yakima River Basin, Washington, USA*. https://data.ess-dive.lbl.gov/view/doi:10.15485/1892052

Gaines, R., & Priestas, A. (2016). *Particle Size Distributions of Bed Sediments along the Mississippi River, Grafton, Illinois to Head of Passes, Louisiana, November 2013.* https://doi.org/10.13140/RG.2.1.2492.1207

Glaser, C., Zarfl, C., Rügner, H., Lewis, A., & Schwientek, M. (2020). Analyzing Particle-Associated Pollutant Transport to Identify In-Stream Sediment Processes during a High Flow Event. *Water*, *12*(6), Article 6. https://doi.org/10.3390/w12061794

Gomez-Velez, J. D., & Harvey, J. W. (2014). A hydrogeomorphic river network model predicts where and why hyporheic exchange is important in large basins. *Geophysical Research Letters*, *41*(18), 6403–6412. https://doi.org/10.1002/2014GL061099

Gomez-Velez, J. D., Harvey, J. W., Cardenas, M. B., & Kiel, B. (2015). Denitrification in the Mississippi River network controlled by flow through river bedforms. *Nature Geoscience*, *8*(12), Article 12. https://doi.org/10.1038/ngeo2567

Harvey, B. N., Johnson, M. L., Kiernan, J. D., & Green, P. G. (2011). Net dissolved inorganic nitrogen production in hyporheic mesocosms with contrasting sediment size distributions. *Hydrobiologia*, *658*(1), 343–352. https://doi.org/10.1007/s10750-010-0504-4

He, K., Zhang, X., Ren, S., & Sun, J. (2014). *Spatial Pyramid Pooling in Deep Convolutional Networks for Visual Recognition* (Vol. 8691, pp. 346–361). https://doi.org/10.1007/978-3-319-10578-9_23

Lang, N., Irniger, A., Rozniak, A., Hunziker, R., Wegner, J. D., & Schindler, K. (2021). GRAINet: Mapping grain size distributions in river beds from UAV images with convolutional neural networks. *Hydrology and Earth System Sciences*, *25*(5), 2567–2597. https://doi.org/10.5194/hess-25-2567-2021

Lepesqueur, J., Hostache, R., Martínez-Carreras, N., Montargès-Pelletier, E., & Hissler, C. (2019). Sediment transport modelling in riverine environments: On the importance of grain-size distribution, sediment density, and suspended sediment concentrations at the upstream boundary. *Hydrology and Earth System Sciences*, *23*(9), 3901–3915. https://doi.org/10.5194/hess-23-3901-2019

Lin, C.-P., Wang, Y.-M., Tfwala, S. S., & Chen, C.-N. (2014). The Variation of Riverbed Material due to Tropical Storms in Shi-Wen River, Taiwan. *The Scientific World Journal*, *2014*, e580936. https://doi.org/10.1155/2014/580936

Menting, F., Langston, A. L., & Temme, A. J. A. M. (2015). Downstream fining, selective transport, and hillslope influence on channel bed sediment in mountain streams, Colorado Front Range, USA. *Geomorphology*, *239*, 91–105. https://doi.org/10.1016/j.geomorph.2015.03.018

Mori, N., Debeljak, B., Kocman, D., & Simčič, T. (2017). Testing the influence of sediment granulometry on heterotrophic respiration with a new laboratory flow-through system. *Journal of Soils and Sediments*, *17*(7), 1939–1947. https://doi.org/10.1007/s11368-016-1613-0

Pebesma, E. (2018). Simple Features for R: Standardized Support for Spatial Vector Data. *The R Journal*, *10*(1), 439–446.

Peterson, R. A. (2021). Finding Optimal Normalizing Transformations via bestNormalize. *The R Journal*, *13*(1), 310–329.

Purinton, B., & Bookhagen, B. (2019). Introducing *PebbleCounts*: A grain-sizing tool for photo surveys of dynamic gravel-bed rivers. *Earth Surface Dynamics*, *7*(3), 859–877. https://doi.org/10.5194/esurf-7-859-2019

R Core Team. (2021). *R: A Language and Environment for Statistical Computing, Vienna, Austria* [Computer software].

Redmon, J., Divvala, S., Girshick, R., & Farhadi, A. (2016). *You Only Look Once: Unified, Real-Time Object Detection* (arXiv:1506.02640). arXiv. https://doi.org/10.48550/arXiv.1506.02640

Regier, P., Chen, Y., Son, K., Bao, J., Forbes, B., Goldman, A. E., Kaufman, M. H., Rod, K. A., & Stegen, J. C. (2023). *Data associated with "Machine learning photogrammetric analysis of images provides a scalable approach to study riverbed grain size distributions"* [dataset]. ESS-DIVE. https://data.ess-dive.lbl.gov/view/doi%3A10.15485%2F1972232

Ren, H., Hou, Z., Duan, Z., Song, X., Perkins, W. A., Richmond, M. C., Arntzen, E. V., & Scheibe, T. D. (2020). Spatial Mapping of Riverbed Grain-Size Distribution Using Machine Learning. *Frontiers in Water*, *2*. https://www.frontiersin.org/articles/10.3389/frwa.2020.551627

Rickenmann, D., & Recking, A. (2011). Evaluation of flow resistance in gravel-bed rivers through a large field data set. *Water Resources Research*, *47*(7). https://doi.org/10.1029/2010WR009793

Schwarz, G. E., Jackson, S. E., & Wieczorek, M. E. (2018). *Select Attributes for NHDPlus Version 2.1 Reach Catchments and Modified Network Routed Upstream Watersheds for the Conterminous United States* [dataset]. U.S. Geological Survey. https://doi.org/10.5066/F7765D7V

Serbin, S. P., Giangrande, S. E., Kuang, C., Urban, N., & Pouchard, L. (2021). *AI to Automate ModEx for Optimal Predictive Improvement and Scientific Discovery* (AI4ESP-1119). Artificial Intelligence for Earth System Predictability (AI4ESP) Collaboration (United States). https://doi.org/10.2172/1769662

Snelder, T. H., Lamouroux, N., & Pella, H. (2011). Empirical modelling of large scale patterns in river bed surface grain size. *Geomorphology*, *127*(3), 189–197. https://doi.org/10.1016/j.geomorph.2010.12.015

Son, K., Fang, Y., Gomez-Velez, J. D., & Chen, X. (2022). Spatial microbial respiration variations in the hyporheic zones within the Columbia River Basin. *Journal of Geophysical Research: Biogeosciences*, *n/a*(n/a), e2021JG006654. https://doi.org/10.1029/2021JG006654

Splinter, D. K., Dauwalter, D. C., Marston, R. A., & Fisher, W. L. (2010). Ecoregions and stream morphology in eastern Oklahoma. *Geomorphology*, *122*(1), 117–128. https://doi.org/10.1016/j.geomorph.2010.06.004

Stähly, S., Friedrich, H., & Detert, M. (2017). Size Ratio of Fluvial Grains' Intermediate Axes Assessed by Image Processing and Square-Hole Sieving. *Journal of Hydraulic Engineering*, *143*(6), 06017005. https://doi.org/10.1061/(ASCE)HY.1943-7900.0001286

Steer, P., Guerit, L., Lague, D., Crave, A., & Gourdon, A. (2022). Size, shape and orientation matter: Fast and automatic measurement of grain geometries from 3D point clouds. *EGUsphere*, 1–31. https://doi.org/10.5194/egusphere-2022-75

Stroud Water Research Center. (2023). *Model My Watershed* [Computer software]. Available from https:wikiwatershed.org

Tremblay, P., Leconte, R., Jay Lacey, R. W., & Bergeron, N. (2014). Multi-day anchor ice cycles and bedload transport in a gravel-bed stream. *Journal of Hydrology*, *519*, 364–375. https://doi.org/10.1016/j.jhydrol.2014.06.036

Wang, C.-Y., Liao, H.-Y. M., Yeh, I.-H., Wu, Y.-H., Chen, P.-Y., & Hsieh, J.-W. (2019). *CSPNet: A New Backbone that can Enhance Learning Capability of CNN* (arXiv:1911.11929). arXiv. https://doi.org/10.48550/arXiv.1911.11929

Wang, J.-P., François, B., & Lambert, P. (2017). Equations for hydraulic conductivity estimation from particle size distribution: A dimensional analysis. *Water Resources Research*, *53*(9), 8127–8134. https://doi.org/10.1002/2017WR020888

Ward, A. S., Wondzell, S. M., Schmadel, N. M., Herzog, S., Zarnetske, J. P., Baranov, V., Blaen, P. J., Brekenfeld, N., Chu, R., Derelle, R., Drummond, J., Fleckenstein, J. H., Garayburu-Caruso, V., Graham, E., Hannah, D., Harman, C. J., Hixson, J., Knapp, J. L. A., Krause, S., … Wisnoski, N. I. (2019). Spatial and temporal variation in river corridor exchange across a 5th-order mountain stream network. *Hydrology and Earth System Sciences*, *23*(12), 5199–5225. https://doi.org/10.5194/hess-23-5199-2019

Wolman, M. (1954). A method of sampling coarse river-bed material. *Eos, Transactions American Geophysical Union*, *35*(6), 951–956. https://doi.org/10.1029/TR035i006p00951

Xia, X., Jia, Z., Liu, T., Zhang, S., & Zhang, L. (2017). Coupled Nitrification-Denitrification Caused by Suspended Sediment (SPS) in Rivers: Importance of SPS Size and Composition. *Environmental Science & Technology*, *51*(1), 212–221. https://doi.org/10.1021/acs.est.6b03886

Zambrano-Bigiarini, M. (2013). *HydroGOF: Goodness-of-Fit Functions for Comparison of Simulated and Observed Hydrological Time Series* [R]. https://github.com/hzambran/hydroGOF

Zhang, W., Itoh, K., Tanida, J., & Ichioka, Y. (1990). Parallel distributed processing model with local space-invariant interconnections and its optical architecture. *Applied Optics*, *29*(32), 4790–4797. https://doi.org/10.1364/AO.29.004790

Supplemental Information associated with “Machine learning photogrammetric analysis of images provides a scalable approach to study riverbed grain size distributions”.

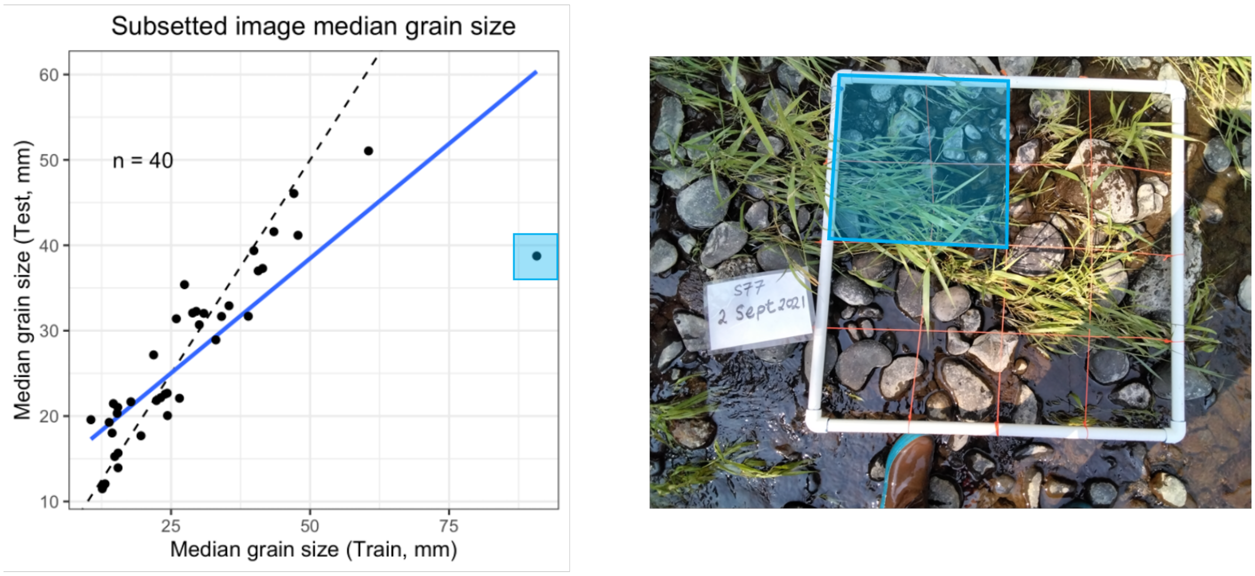

Figure S1: Figure 2B including one outlier that was removed prior to fit and error analysis. Both the outlier and the corresponding spatial extent within the training image are both highlighted in blue.

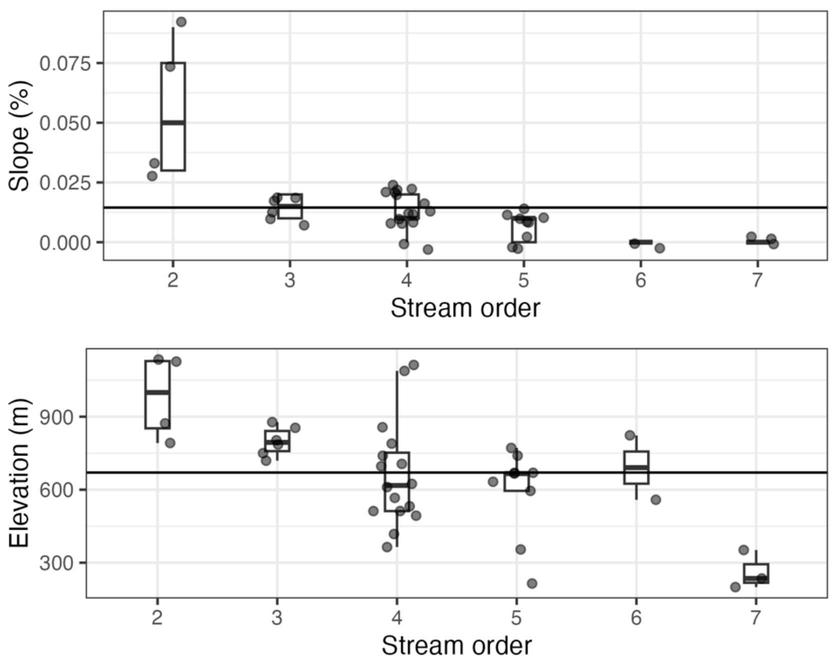

Figure S2: Catchment-scale site characteristics (average slope and elevation) by stream order.

801

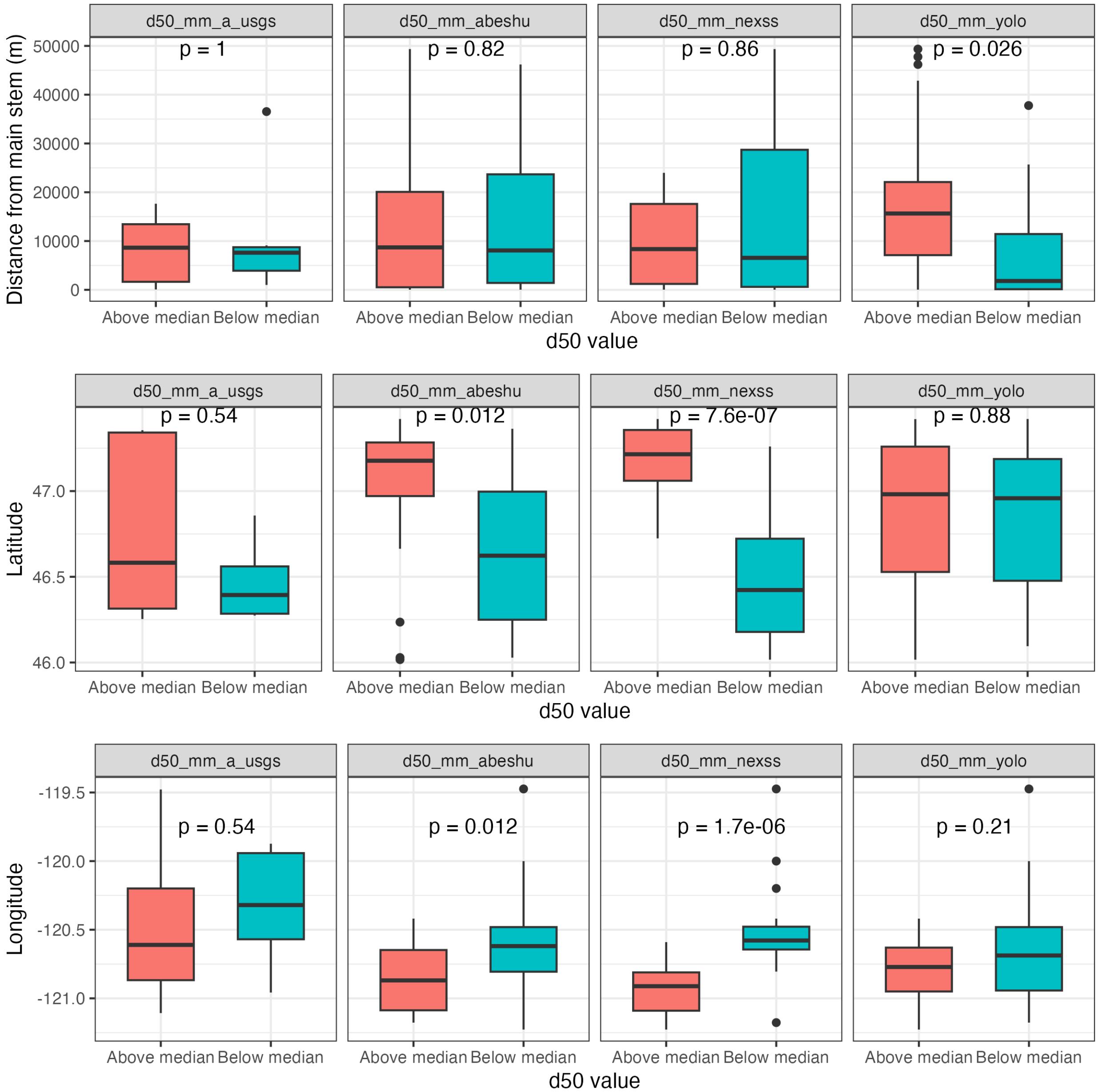

802 Figure S3: Boxplots that present statistics that accompany Figure 4. A) Straight-line distance in
803 m of sites from the main stem of the Yakima, as shown in Figure 4, B) site latitude, and C) site
804 longitude. Differences between means are presented as p-values, where significance is
805 determined as $p < 0.05$.
806
807

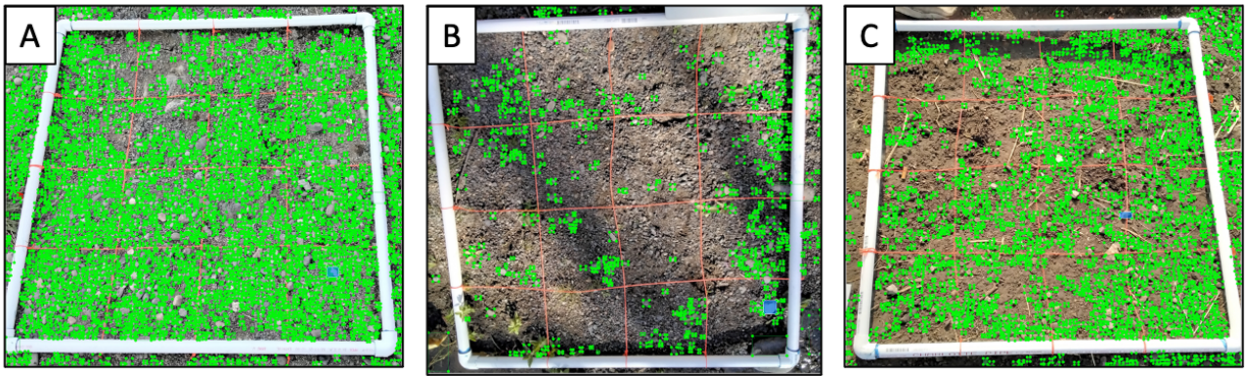

Figure S4: The photos corresponding to the outliers in the “Yes” group highlighted in Figure 7.

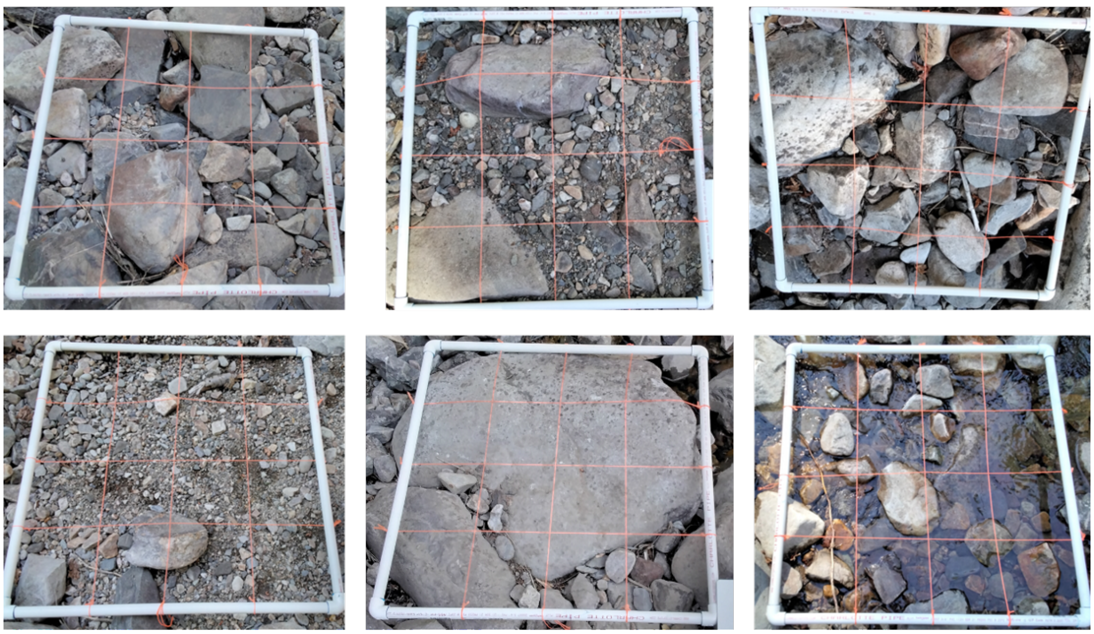

Figure S5: The 6 photos for Site 15.

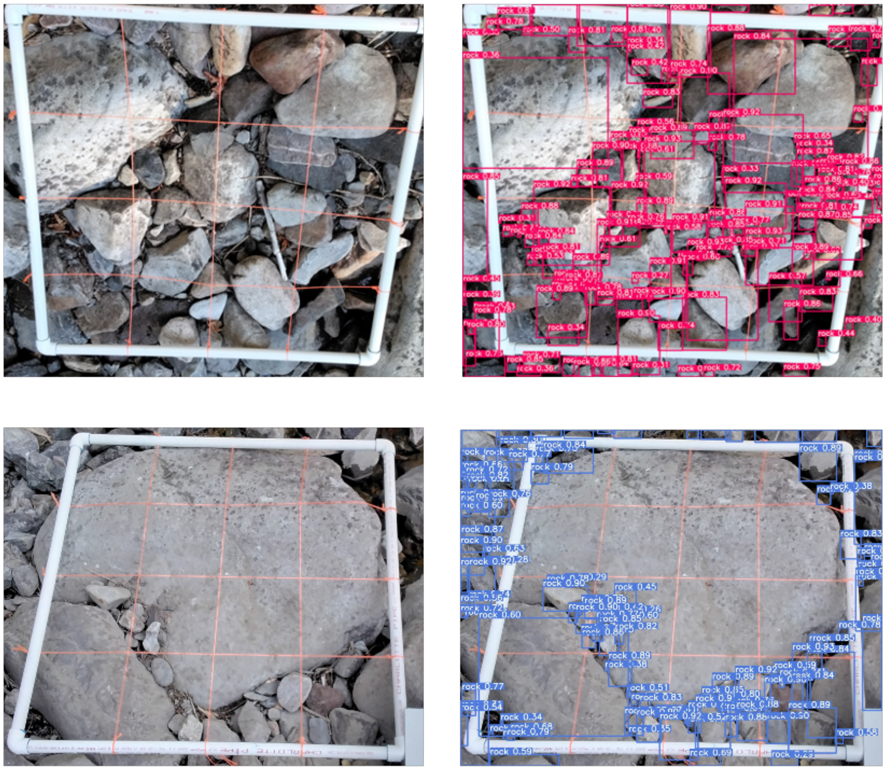

Figure S6: Comparison of the raw photo and YOLO prediction for photo C (upper row) and E (lower row).